GEOPRESSURE ANALYSIS AND RESERVOIR FLUID DISCRIMINATION IN A CENTRAL SWAMP FIELD, NIGER DELTA, NIGERIA

K. K. Nwozor[1, 2], L. O. Onuorah[3]

[1]*Department of Geology and Petroleum Geology, University of Aberdeen, Aberdeen, United Kingdom;*[2]*Department of Geology, Chukwuemeka Odumegwu-Ojukwu University, Uli, Nigeria;*[3]*Department of Physical and Geosciences, Godfrey Okoye University, Ugwu-omu Nike, Nigeria;* Correspondence*: kknwozor@yahoo.com*

Abstract

Significant discrepancies often exist between measured and predicted pore pressures especially in deep-seated reservoirs in the Niger Delta Basin. The associated risks when not properly considered contribute to drilling challenges and some exploration downturns. At the background to these challenges is the vague understanding of the subtle complexities that may characterize the geopressure system. Key to this is the growing need to account for additional mechanisms of overpressure generation beyond the routinely believed undercompaction during pressure prognosis and well planning. Data from a deep well in the Central Swamp Depobelt depict the occurrence of two vertical effective stress regimes. The corresponding two pressure settings are separated by massive succession of shales at an approximate depth of 14500ft (4421m) towards the base of the Agbada Formation. Cross-plots of density and velocity as well as velocity and vertical effective stress indicate that undercompaction dominates pressure generation above the massive shale while late geopressure processes, especially hydrocarbon generation could be responsible for deep-seated extreme overpressures. The intervening massive shale acts as an effective regional seal with the result that there is no pressure communication between the reservoirs above and beneath it. Calculated overpressures in the water-saturated section of the reservoir that lies above the seal typically were below 150 psi (1.03MPa). On the contrary, overpressure beneath the seal is as much as 4490psi (30.96MPa). Pressure estimation based on standard Eaton method failed to produce matching profile with measured data in the deep reservoir. Modified Eaton and Bowers methods were then used to obtain a geopressure profile consistent with wireline measurements.

Key words: Geopressure; unloading; petrophysics; fluid determination; Niger Delta.

1. Introduction

Major decisions on projects are driven by the economics and sustainability of such ventures. Exploration and development of oil and gas resources require well informed decisions to guide well planning, drilling logistics and sustainable development of target prospects. Critical to all these is adequate understanding of formation pressures and nature of fluids in the target reservoir especially as focus of drilling campaigns continues to shift towards deep-seated high-pressure high temperature (HPHT) deposits.

Exploration needs geopressure knowledge for accurate interpretation of relevant subsurface data and formation characterization. There are worldwide examples of costly wells that could not produce because the target reservoirs were found to contain only residual hydrocarbons as a result of fluid losses through fractures initiated in the bounding seals by extreme high formation pressures. Drilling campaigns require reliable estimates of formation pressures in order to adequately design wells and apply the right drilling mud weights for optimal project delivery. Pressure-related drilling challenges include kicks and influxes, borehole instability, tool sticking, poor returns of drilling fluids and often blowouts. As a consequence, inappropriate drilling programme could damage the formation and render the target reservoir inoperable. The quantification and management of pore pressures greatly impact on the prospect throughout its entire life cycle from exploration to production and depletion. In this paper, recent knowledge

is applied using well data to evaluate overpressure trends and causative mechanisms in a field located in the Central Swamp Depobelt of the Niger Delta Basin.

2. Geologic setting of study area

The Niger Delta oil province is located in the Nigeria sector of the Gulf of Guinea. Sediments in the Niger Delta have been deposited from Paleocene times until present day. Comprehensive summaries of the geological history, tectono-stratigraphic setting and hydrocarbon habitat of the Niger Delta can be found in Weber and Daukoru [21], Doust and Omatsola [7]. The structural patterns mainly indicate that the delta comprises six depobelts (Figure 1) that include the Central Swamp where the study area is located. These depobelts contain characteristic sedimentary and structural styles developed during repeated phases of delta tectonism and associated sedimentary responses.
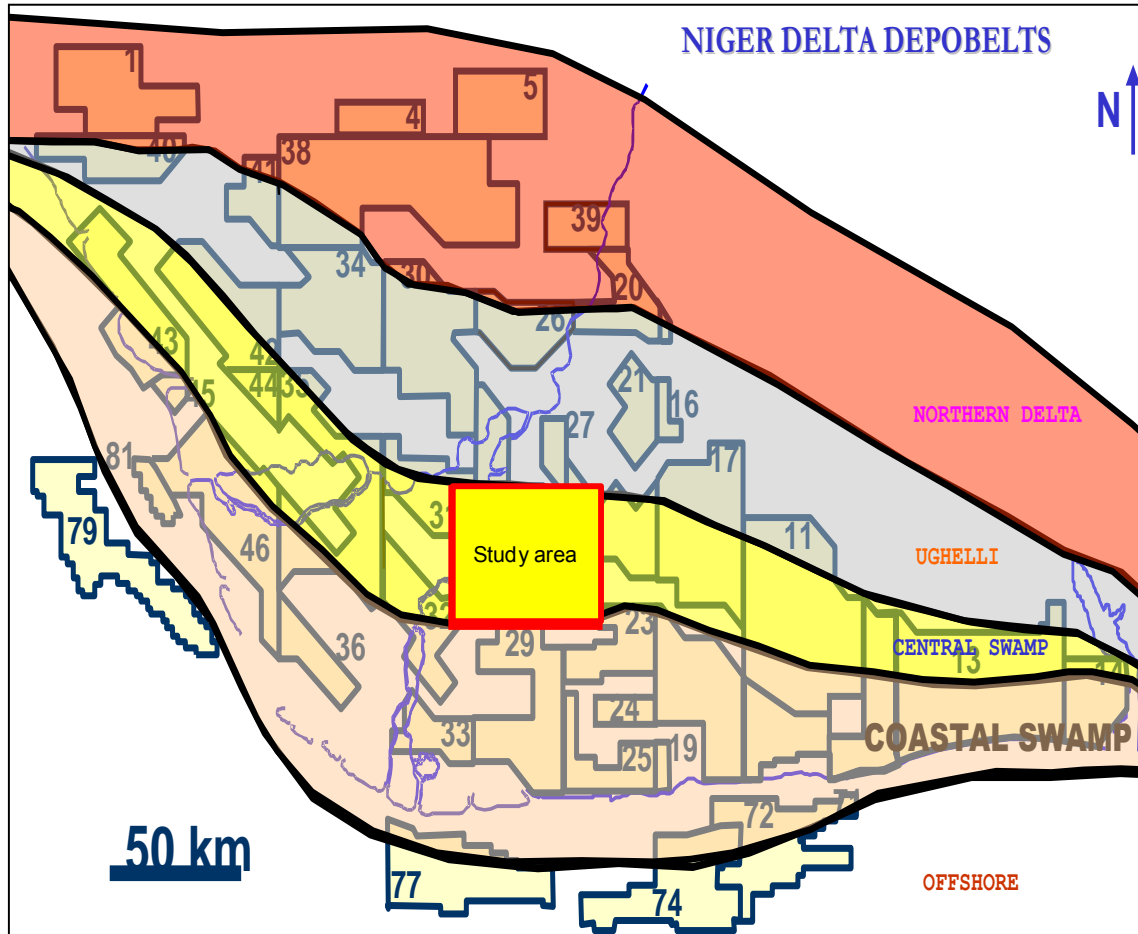

Figure 1 Section map of Niger Delta showing main depobelts and oil prospecting leases. The study area (red box) situates in the Central Swamp Depobelt (modified from [9]).

The Tertiary stratigraphic succession (Figure 2) is usually subdivided into three lithostratigraphic units namely the Benin Formation, Agbada and Akata Formations. The youngest of the succession, the Benin Formation consists of massive continental, river-deposited gravels and sands that could be as much as 2000 metres in thickness. Underlying Benin Formation is the paralic Agbada Formation which in itself is a massive interfingering of marine and continental sediments with thickness often in excess of 5000 metres. It is made up of interbedded fluviatile, coastal, fluviomarine sands and marine shales. The oldest in the succession is the Akata Formation that consists of massive thicknesses of marine shales or clays with stringers of sands and silt. This succession corresponds to the frequently used classification into continental, transitional, paralic and marine depositional environments.
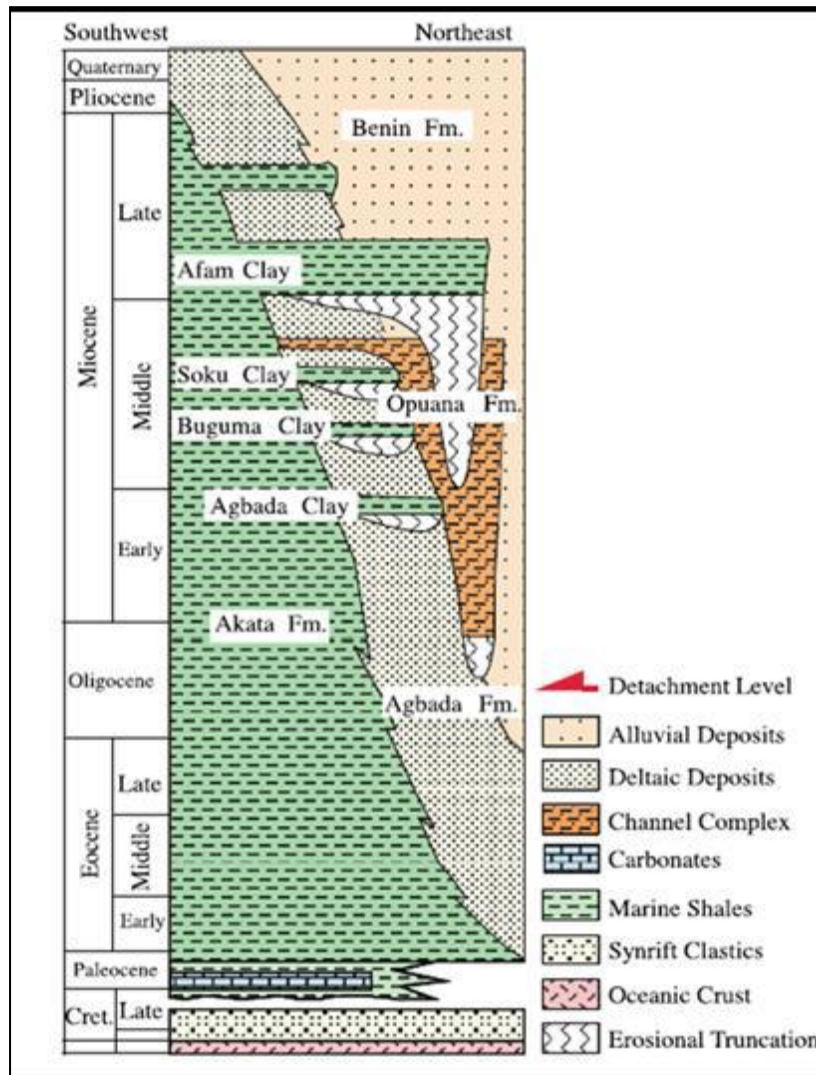
Figure 2 A regional schematic illustration of the main stratigraphic units in the Niger Delta Basin (Source: Corredor *et al.*, [5])

2.1 Niger Delta Geopressure system

Operational experience in the Niger Delta gives insight that its geopressure system is reflective of its stratigraphy and structuration. The sand–dominated unconsolidated sediments of the Benin Formation maintains free hydraulic communication with the surface and are thus in normal hydrostatic equilibrium. The development of massive regional shales in sections of Agbada Formation begins to alter this normal pressure state with the implication that pockets of encased sands in the sand-shale succession could exhibit various degrees of rising fluid pressures. Many geopressure studies are able to forecast pore pressures with ease in these intervals because they are mainly as a result of stress-controlled undercompaction. Complexities to pressure prognosis often arise when overpressured fluids have been remobilised through the numerous fault systems and connected channel complexes in the area with the implication of unexpected drilling challenges, costly well abandonments and unproductive reservoirs. At deeper settings of the Niger Delta petroleum system are the source rocks of the Akata Formation. These are massive thickness of organic-rich shales that are believed to feed hydrocarbons to encased sands and reservoirs of the Agbada Formation. Temperature-dependent source rock diagenesis and hydrocarbon maturation process may generate high overpressures that are often experienced in some deep wells. Encountering such high magnitudes of overpressure traditionally leads to termination of such wells while the shallower less overpressured reservoirs are exploited. As a new wave of HPHT campaigns begin in the Niger Delta, a new look at formation and resource evaluation becomes necessary.

2.2 Well history

The study utilized data from a vertical exploration well that situate in the Central Swamp depobelt of the Niger Delta basin. Drilled on a derrick floor elevation (DFE) of 62.7ft (19.12ft), this overpressured well has a total depth of 16020 ftss (4884m). The target reservoirs are mainly multiple layers of barrier bar deposits as well as tidal and distributary channels that are discretely sealed by massive shales (Table 1).

Table 1 Formation tops and marker beds established from well log

Formation	Top (ftss)	Base (ftss)	Dominant lithology
Benin Formation	Surface	7237	Continental sands inter-bedded with claystones and lignite
	7237	8837	Massive shales and graded sandstones
Agbada Formation	8837	11571	Prodelta shales inter-bedded with silty sands
	11571	12461	Micaceous silty shales, siltstones & calcareous sandstones
	12461	14531	Massive sand sequence inter-bedded with silty shales
	14531	15951	Thin silty calcareous sandstone and massive blocky shale
Akata Formation	Not reached	N/A	Continuous source rock shales

Reservoir Formation Test (RFT) data show minor increases in pore pressures from 0.444psi/ft at 11717ft (3572.3m) to 0.463psi/ft at 15233 ft (4644.2m) and continued till 15716ft (4791.5m) when a sudden ramp to 0.72psi/ft was observed after drilling through a 100ft thickness of shale and penetrating a sand column. This was followed by rapid rise in gas levels of up to 78% and a subsequent drill break and kick that was killed with a 0.74psi/ft. Drilling to the target depth was achieved using a mudweight of 0.75psi/ft. The main structure in the field is formed by a large east-west trending rollover anticline and a major syn-sedimentary fault that dips to the south.

3. Materials and method

Available data were wireline logs such as gamma-ray, density, sonic, resistivity and calliper. Drilling data include mudlogs, composite logs and formation test results while relevant events, depth and stratigraphic checks were obtained in well reports. Relevant data were collated from applicable sources and edited accordingly. For instance, wireline logs were plotted and examined for gaps, spikes and poor wellbore conditions using calliper log readings. Data within bad sections of the well were excluded from the study and interpolations made where necessary. Available formation test results were given as repeat formation test (RFT) and these were first quality-checked based on logger's positive comments in well files. Since such measurements can only be obtained in permeable sands, a depth plot was made alongside gamma-ray to pin-point that the source depth-points are actually in the sands. Considering that some radioactive sands could exist in the Niger Delta, identified sand intervals were cross-checked in the composite logs. The influence of temperature was investigated using a combination of published regressions such as 27 °C / km and measured formation temperatures found in well reports.

Plots of all carefully edited data were made and subsequently interpreted for the results discussed in this study. Overburden stress was first calculated using a combination of density logs in logged sections and Athy's equation in non-logged zones. Since pore pressure prediction is done in shales, carefully edited properties of continuous shale layers were built into a shale trend suing the RokDoc software. These were evaluated for deviations from normal trends. The need to work with reliable hard data made it necessary to use continuous trends of shale properties through encased sands. Thus, measured pressure points and their derivatives were cross-plotted with corresponding shale trend across the interval. Through depth plots of pressure and overpressure, we aim to note the presence of overpressures. With crossplots of shale velocity and vertical effective stress, we decide mechanisms that generate observed overpressures and our predictive strategy. We then take a more detailed look at overpressure-

depth plots for gradient differences that could be indicative of varying fluid densities and fluid types.

3.1 Data analysis

Pressure gradients derived from the tests were used to estimate formation fluid properties. The need to work with overpressures rather than just pressure magnitudes informed the determination of normal hydrostatic pressures in the field. This was done by extracting measured pore pressures in unrestricted free-draining formations (Table 2) and plotted (Figure 3) in order to establish a data-constrained approximation for the hydrostatic pressure gradient in the area. A baseline value of 0.4299psi/ft was obtained and used in calculating amounts of overpressure in measured intervals of the wells. This is shown below:

Table 2 Measured pore pressure data in freely-draining aquifers in the field.

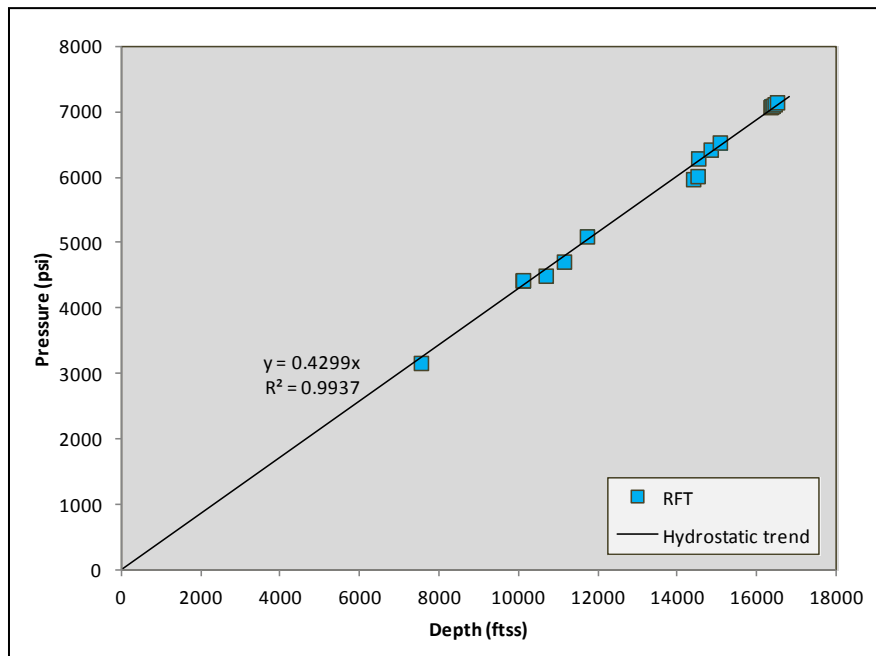| Depth TVDss (ft)	Depth TVDss (m)	MPP (psi)	MPP gradient (psi/ft)	Comment	Wells
7535.81	2297.503	3161	0.419	Hydrostatic	a
10096.58	3078.226	4422	0.438	Hydrostatic	b
10107.54	3081.567	4427	0.438	Hydrostatic	b
14519.50	4426.677	6289	0.433	Hydrostatic	c
14833.50	4522.409	6424	0.433	Hydrostatic	c
15063.50	4592.53	6533	0.434	Hydrostatic	c
16339.50	4981.555	7074	0.433	Hydrostatic	c
16360.50	4987.957	7084	0.433	Hydrostatic	c
16393.50	4998.018	7094	0.433	Hydrostatic	c
16443.50	5013.262	7117	0.433	Hydrostatic	d
16503.50	5031.555	7148	0.433	Hydrostatic	d
10679.00	3255.793	4495.9	0.421	Hydrostatic	d
11138.00	3395.732	4711.4	0.423	Hydrostatic	d
11717.00	3572.256	5096.9	0.435	Hydrostatic	d
14391.00	4387.5	5972.3	0.415	Hydrostatic	d
14503.00	4421.646	6018.75	0.415	Hydrostatic	d
	Average		0.429	Hydrostatic	

Figure 3 Plot of measured pore pressures in freely draining aquifers for the determination of suitable hydrostatic pressure baseline in the field. A gradient of 0.4299psi/ft (≈0.43psi/ft) was calculated for hydrostatic pressures and was used as the basis for quantifying excess pressures in the field.

3.2 Determination of overburden stress

Overburden pressure at any depth is the pressure that results from the combined weight of the rock matrix and the fluids in the pore space overlying the formation of interest. The difference between this value and vertical effective stress (pressure acting on the solid rock framework) is pore pressure. It is important to evaluate overburden stress early in geopressure analysis because it is a phase of the workflow that involves all rock types (not only shales). Beyond this estimation, other iterations in pore pressure studies commonly make progress with shale property trends. The overburden stress was calculated from density log using bulk rock density data from surface to target depth in the subsurface using the Engelder [10] method:

$$\sigma_v = \sum \rho_{(z)} g h \tag{1}$$

where: σ_v = overburden / lithostatic / geostatic / total vertical stress; $\rho_{(z)}$ = bulk density of the overlying sediment matrix at specified depth z ; g = acceleration due to gravity (9.81 m/s); h = thickness of unit rock layer

A major challenge of working with density logs is that it is rare to have them completely run along the entire well path (Figure 4). Unlogged sections of the well were filled up using Athy's [1] porosity exponential model of the form:

$$OBP = 0.4335 * \left[\rho_{mat} z - \frac{\phi_{crit}}{C} \left(\rho_{mat} - \rho_{water} \right) \left(1 - e^{(-c*zgl)} \right) \right] \tag{2}$$

where OBP is the overburden stress; ρ_{mat} is the matrix density; and ρ_{water} is the water density; ϕ_{crit} is the critical or surface porosity and C is the compaction factor; and z is vertical depth.
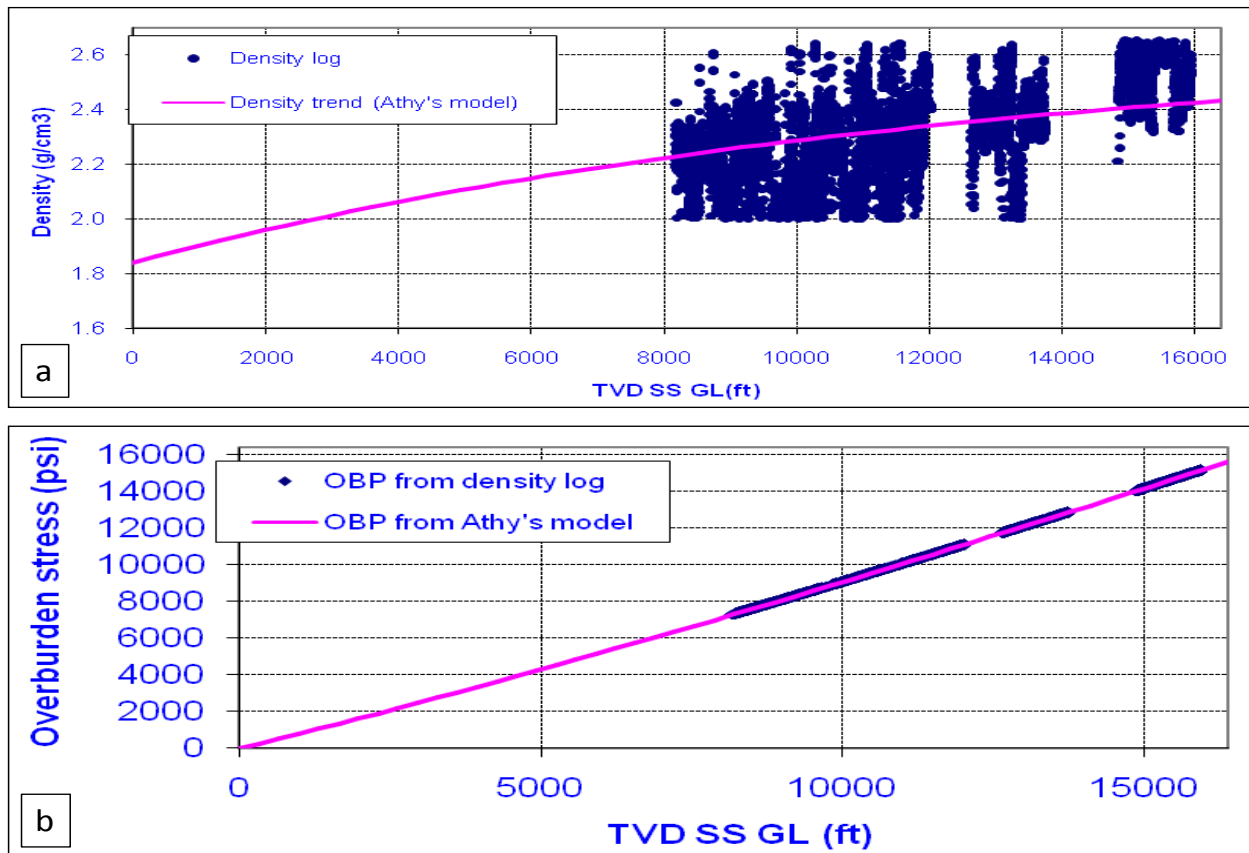

Figure 4 Density logs (a) were used for the calculation of overburden stress (b). Short run length of the log necessitated the use of Athy's formula to fill missing sections.

3.3 Pressure generating mechanisms

Pore pressure is defined as the pressure acting on the fluids in the pore space of a formation. This pore fluid pressure equals the hydrostatic pressure of a column of formation water extending

to the surface and is also called normal pressure. Overpressure occurs when pore pressure exceeds normal hydrostatic pressure and is related to certain environmental conditions in a given earth section. These causative factors could be stress-driven undercompaction that results from ineffective dewatering of compacting sediments. In some severe situations, tempe- rature- dependent processes such as hydrocarbon generation and clay diagenesis could aggravate overpressure development. Details of pressure generating mechanisms and there recognition abound in literature such as Yardley and Swarbrick [22], Swarbrick et al., [17]; O'Connor et al. [16]; and Zhang [23]. Disequilibrium compaction, as a source of overpressure is believed to be active in the Niger Delta. However, Nwozor et al., [15] and Chukwuma et al. [6] have presented evidence of additional mechanisms beyond undercompaction.

In order to determine an accurate pore pressure estimation strategy, depth plots of shale-only logs and cross-plots of various shale rock properties were made. Petrophysical logs (Figure 5) such as sonic, density, resistivity and porosity can be used in recognising changes in formation pressures. This is possible because of the relationship between compaction and measurable rock properties on log. Under conditions of slow burial, normal compaction of sediments occurs. This process of compaction rate that equals rate of dewatering continues until the mechanical process of compaction is hindered by either the stiffness of the rock frame or by increases in pore pressure that retard further compaction. If the rate of compaction exceeds the rate at which fluid can be expelled from the pore space, or if dewatering is prevented by the accumulation of low permeability sediments and formation of seals during burial, the pore fluid begins to support part of the overburden load and consequently becomes overpressured. This primary process of overpressure generation is known as disequilibrium compaction or undercompaction.
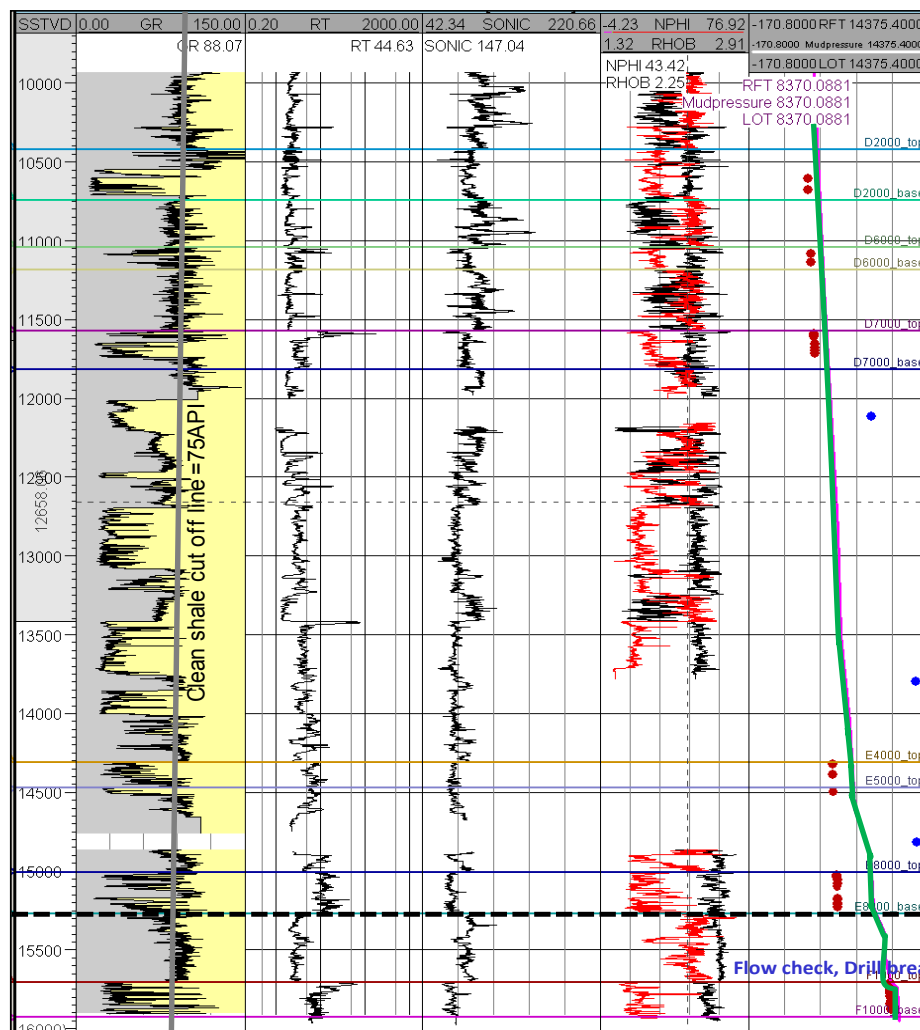

Figure 5 Plot of edited logs and drilling data used in the study. Gaps in logs could be due to washouts and tool limitations.

Temperature increase alters sediments leading to the generation of high overpressures in such processes that may include unloading and load transfer.The increase in fluid pressures retards the compaction process causing a reduction in the grain contact stress (VES), which causes the velocity to decrease significantly with depth while density may remain unchanged thus producing the classic signature of unloading. Crossplot of sonic velocity versus density (Figure 6) have been used to recognize the effect of secondary mechanisms of overpressure generation in the study area. The scatter in the plot data may be indicative of varying qualities of the discriminated shales. The unloading zone becomes very obvious because of the abrupt decrease in velocity at a constant density below the 14400ft (4390m) depth range.
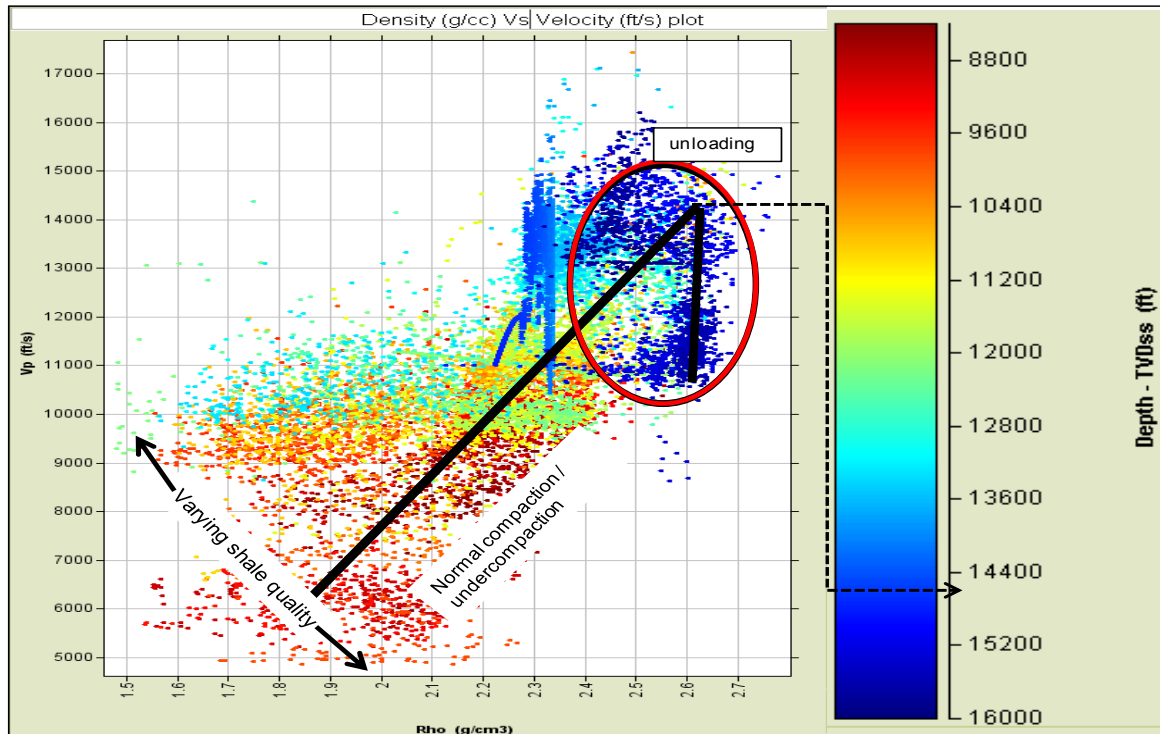

Figure 6 Cross-plot of density and velocity indicates the occurrence of post-undercompaction overpressures

In addition to density versus velocity cross-plot, vertical effective stress was cross-plotted with shale-trend velocity and calculated temperatures based on a regional geothermal gradient of 27°C/km in the Agbada reservoir. VES at this stage was obtained as difference between calculated overburden stress and measured pore pressure. Corresponding velocity is interpolated shale trend that runs from shales atop and below the encased reservoir sands where pressure measurements took place. This data is shown in Table 3 below:

Table 3 Measured reservoir pressure data, calculated VES and temperature with corresponding shale trend velocity

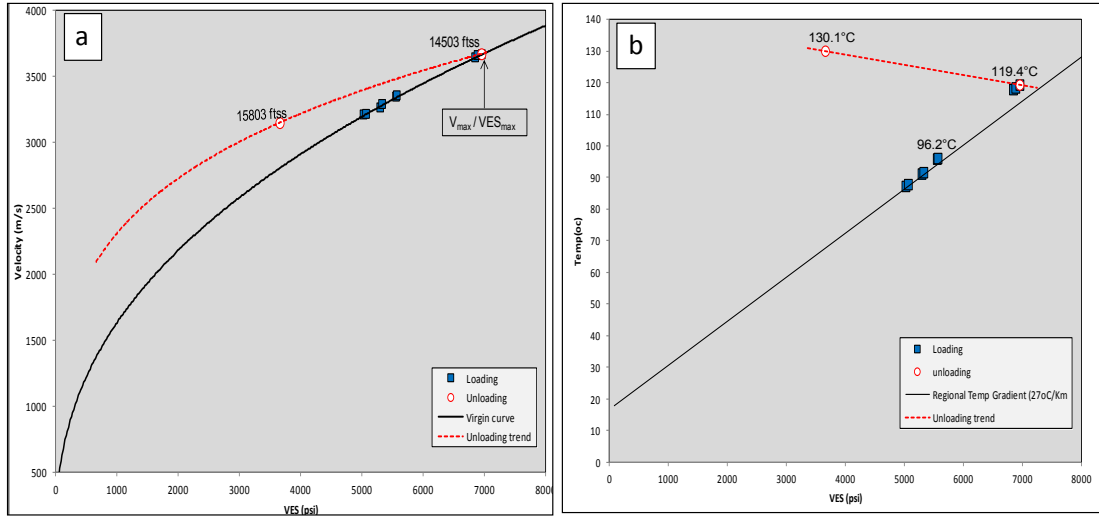| Depth(ftss)	Depth (m)	MPP (Psi)	OBP (psi)	VES (psi)	Shale_Vp(m/s)	Temp(°C)
10609	3234.451	4658	9677	5019	3215	87.33018
10679	3255.793	4687	9747	5060	3219	87.9064
11086	3379.878	4863	10155	5292	3268	91.25671
11138	3395.732	4885	10207	5322	3294	91.68476
11659	3554.573	5182	10732	5550	3350	95.97348
11682	3561.585	5191	10754	5563	3360	96.1628
14327	4367.988	6623	13465	6842	3648	117.9357
14391	4387.5	6649	13531	6882	3665	118.4625
14503	4421.646	6696	13647	6951	3671	119.3845
15803	4817.988	11350	15005	3655	3149	130.0857

Figure 7 Cross-plots of VES with velocity (a) and temperature (b) indicate significant deviations from established normal regional trends. Therefore, it became necessary to adopt a pressure evaluation strategy that will incorporate secondary mechanisms of overpressure generation. Maximum VES value was calculated at a depth of 14503 ftss. Estimated temperature at this depth is 119.4°C.

Figure 7 shows that velocity progressively increased with VES along the virgin curve until it reached an approximate depth of 14503 ftss (4422m) where a reversal begins to trend a separate curve. This point of reversal corresponds to a temperature regime of 119.4°C which is within the thermal window for hydrocarbon generation and expulsion (Hunt [13]). When considered together with the trend observed in preceding density-velocity cross-plot (Figure 6), it becomes less doubtful that there are significant indications of additional sources of overpressure beyond undercompaction. Interpretations offered in Bowers [2] and Swarbrick [18] suggest that this could be the result of high pressure generation due to hydrocarbon maturation processes and associated load transfer effects. Consequently, conventional methods of pore pressure prediction may not yield accurate results beyond the identified depth of reversal (O'Connor *et al.* [16]).

3.4 Pore pressure analysis

Modified Eaton's and Bowers methods (Bowers [2]) have been adopted in this study as a way of accounting for the observed secondary sources of overpressure. Eaton method is routinely used in the industry to estimate the vertical component of effective stress,σ from sonic/seismic velocities, V using the relation:

$$\sigma = \sigma_{normal}\left(\frac{V}{V_{normal}}\right)^{n} \qquad (3)$$

where σ_{normal} and V_{normal} are the vertical effective stress and velocity that would respectively occur under normal hydrostatic pressure conditions; n is an exponent which describes the sensitivity of velocity to effective stress. Under normal and undercompaction conditions, $n = 3.0$; in instances of unloading, modified Eaton's method involves simple upward adjustment of n to values greater than 3.0 in order to simulate the unloading curve. The resulting pressure transform is of the form:

$$Pp = S - (S - P_{n})\left(\frac{V_{obs}}{V_{nor}}\right)^{n} \qquad (4)$$

where, Pp is the pore pressure, S is the overburden stress; P_{n} is the normal/hydrostatic pressure which was taken as 0.43psi/ft as obtained in this study; V_{obs} and V_{nor} are observed shale velocities on wireline log and theoretical normal value respectively. An Eaton exponent, n, value of 5.5 was used to simulate geopressure profile in the well.

The second geopressure trend was achieved using Bowers [12] method which involves the use of effective stress, normal and unloading curve relations to account for pressure regimes emanating from different sources. Bowers equation is a power law relationship between velocity and effective stress that has been widely applied for interpreting stress and predicting fluid pressure (Huffman *et al.* [12]). The basic equations are:

$$V = V_0 + A\sigma^B \tag{5}$$

and
$$V = V_0 + A * \left(\sigma_{max} * \left(\frac{\sigma}{\sigma_{max}} \right)^{\left(\frac{1}{U} \right)} \right)^B \tag{6}$$

where, V_0 is the velocity of sediment at surface; A and B are the loading curve independent parameters calibrated with sonic velocity versus effective stress data; and U is the unloading curve expression of sediment plasticity. The maximum vertical effective stress may be estimated from this equation as:

$$\sigma_{max} = \left(\frac{V_{max} - V_0}{A} \right)^{\frac{1}{B}} \tag{7}$$

Here, σ_{max} and V_{max} are the estimated values of the effective stress and velocity at the onset of secondary overpressure. V_{max} can be set to be equal to the velocity at the start of velocity reversal.

Pore pressure is thus calculated using Terzaghi [19] effective stress principle:

$$\sigma_{eff} = S - P \tag{8}$$

where σ_{eff} is the vertical effective stress; S is the overburden stress; and P is the pore pressure.

4. Results of pore pressure prediction

The results obtained from log-based pore pressure estimation have been compared with the actual pressure measurements for the well. Figure 8 is a plot of measured and predicted pore pressure trends along the well path as well as the mud weights used in drilling the well. Both measured and predicted pore pressures are seen to be within the constraints of the mud weight until approximately 14500ft. Similarly, pressure prediction based on original Eaton method worked well until the well penetrated top of massive shale at approximately 14500ft; beneath this interval, significant discrepancy exists between pressure profile simulated with original Eaton and measured pore pressures to the extent that formation pressure was underestimated by as much as 2307 psi at 15803 ft. This further indicates that overpressures observed above the massive shale (depths ≤ 14500ft) could be as a result of undercompaction.

Applying Bowers and modified Eaton methods produces a geopressure profile that is consistent with measured pore pressures, mud weight adjustments and reported well events below the massive shale (depths ≥ 14500ft) in the deep section of the well. The mudweight profile shows that formation pressure is well constrained by mud weight until the massive shale was penetrated at approximately 14500ft (4421m) where significant rise in background gas levels depict likely under-balance drilling (Figure 9) which was subsequently controlled by quick-succession rapid increases in mud weights.

4.1 Reservoir fluid discrimination

Hydrocarbons (gas and oil) have lower densities than water and can therefore be identified on depth plots of reservoir pressure data. The quality of natural water varies from fresh to saturated brines and in certain exceptional cases may contain heavier solutes. Typically, pressure gradients of water in aquifers range from 0.434psi/ft to 0.52psi/ft corresponding to fluid densities of 1.00g/cc to 1.20g/cc (Swarbrick *et al.* [17]. The presence of heavier solutes can increase these values to as high as 0.54psi/ft (1.25 g/cc) to 0.55 psi/ft (1.27g/cc) while it could drop significantly at some extreme depths to values lower than 0.434psi/ft (1.001g/cc) due high temperature and high pressure effects. Similarly, normal oil gradients under normal temperature and pressure conditions range from

0.38psi/ft to 0.34psi/ft while gas varies from 0.14psi/ft to 0.10psi/ft; between distinct oil and gas range of values could also plot condensates.
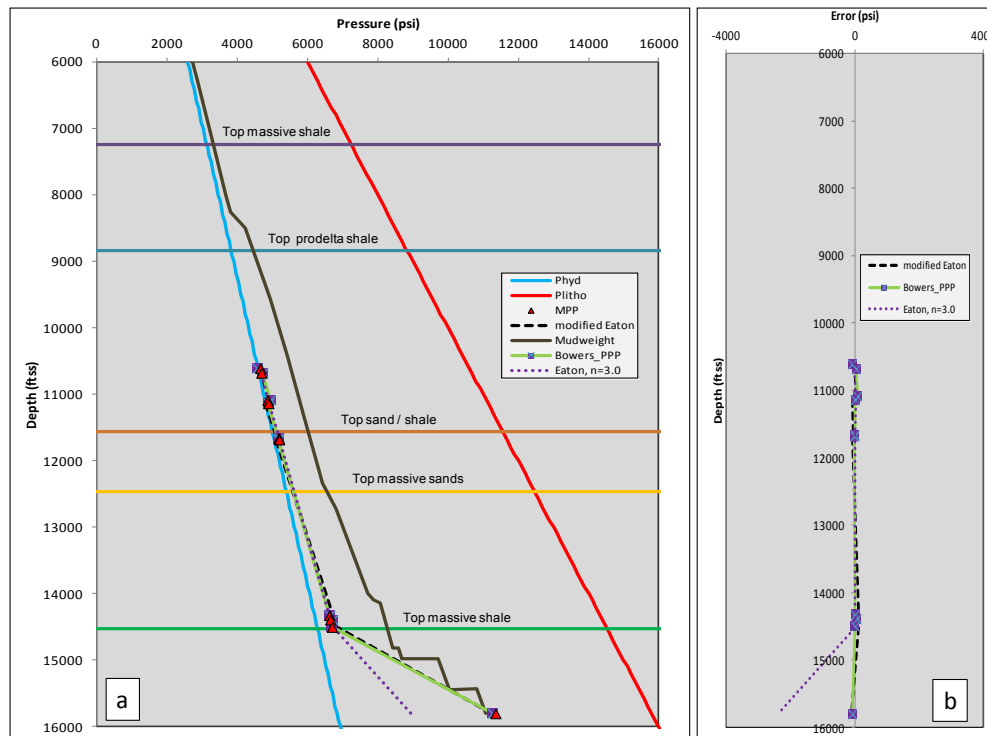

Figure 8 Comparison of wireline pressure data (red triangular dots) with predicted pressures (a) using the three methods and the errors associated with each of the approaches (b). Original Eaton exponent (dotted purple line) under-predicts formation pressures at 15803ft (4818m) by as much as 2391psi (16.49MPa).
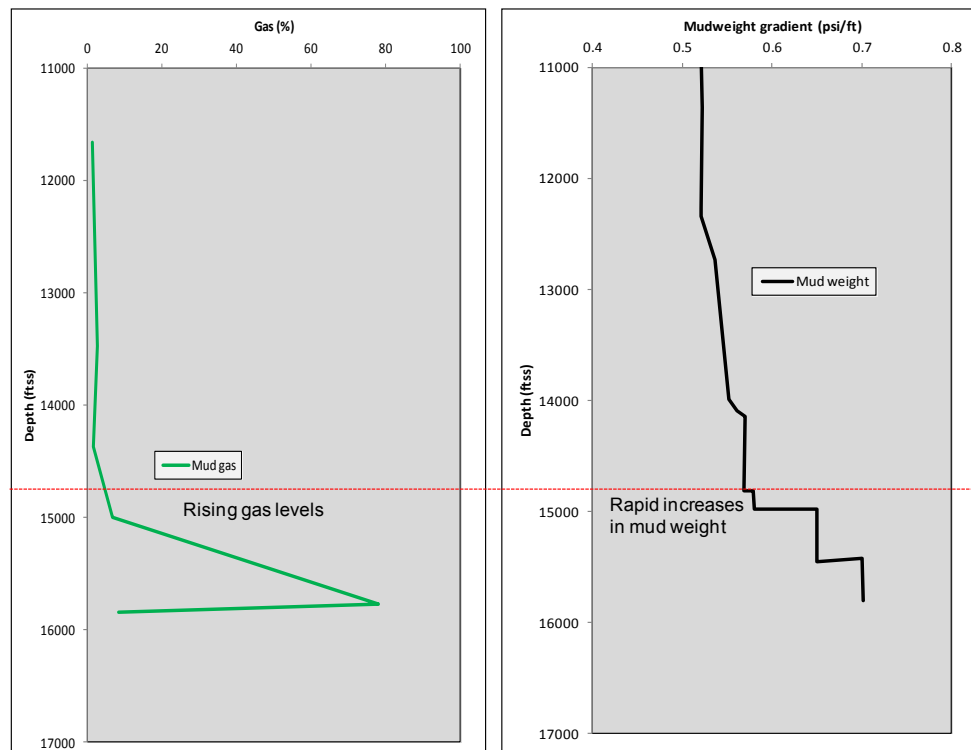

Figure 9 Maximum gas values recorded in mud log. Drilling with inappropriate mud weight leads to gas influx into the wellbore hence the observed high gas values in returning mud at some critical depths

Wireline pressure data were further analysed to determine the nature of fluids in the reservoir. This involved transforming the data to discount the effect of static fluid (pore pressure minus hydrostatic pressure). The static fluid gradient is already evaluated as 0.43psi/ft and presented in Figure 3 and corresponds to a fluid density of 0.992g/cc. A depth plot of derived overpressure amounts makes it possible to establish points of slope changes on the corresponding pressure-depth plot that were diagnostic of differing fluid pressure gradients and contact zones (Figure 10). Converting fluid pressure gradients to densities enables likely fluids to be identified such that free-water-levels could be delineated from their contacts with other fluids present in the reservoir. Detailed workflow for this analysis is as discussed in Brown [4].
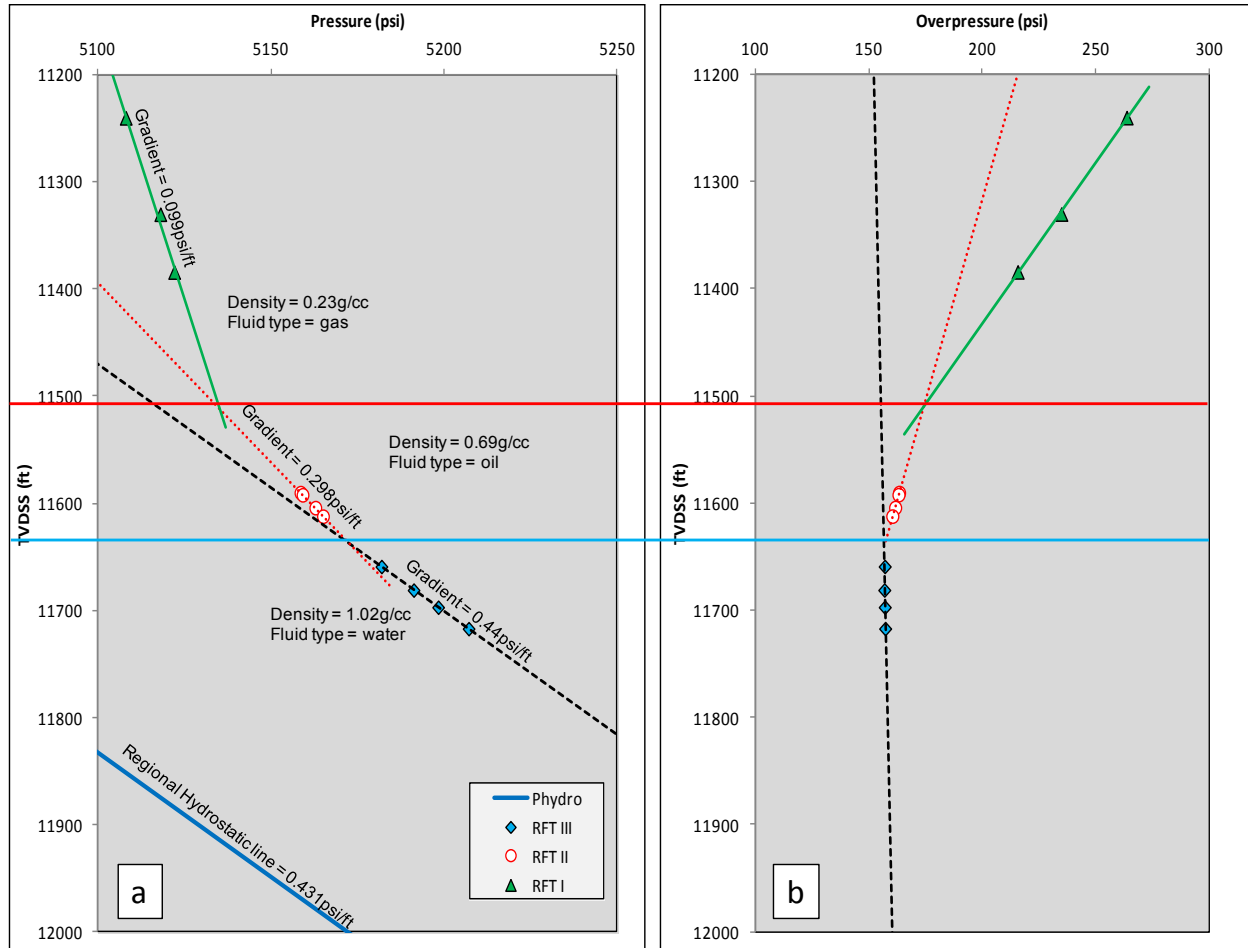

Figure 10 Depth plots of measured pore pressure (a) and overpressure (b) in the upper reservoir section (11200ft to 12000ft). Aquifer pressure has risen above the normal levels by as much as 150 psi.

Figure 10 above makes it possible to recognize three tiers in both pressure trends and overpressure plots. Overpressures calculated using the determined hydrostatic gradient of 0.43psi/ft establishes that the water leg in the reservoir is overpressured by as much as 150psi (1.03MPa) giving a vertical trend at the base of the section. It is overlain by a short diagonal column and a subsequent longer diagonal column. Slope changes in pressure and overpressure depth plots could be as a result of fluid density changes at fluid contacts and across fluid-flow barriers (Brown, 2003). Evident slope changes in Figure 10 occur at approximately 11520 ft (3513m) and 11650ft (3552m). The gradients on pressure-depth plots are 0.44psi/ft, 0.298psi/ft and 0.099psi/ft respectively. Converting fluid pressure gradient to density, the corresponding densities   are 1.02g/cc, 0.69g/cc and 0.23g/cc respectively. Conventional fluid property charts widely recognize that these density values correspond to water, oil and gas respectively. Thus, an oil-water contact (OWC) is at delineated at 11650ft which is the intersection between highest

data on water trend and lowest value on oil slope. Similarly, the intersection of gas and oil data trends indicates that gas-oil contact (GOC) lies on 11520ft (3513m).
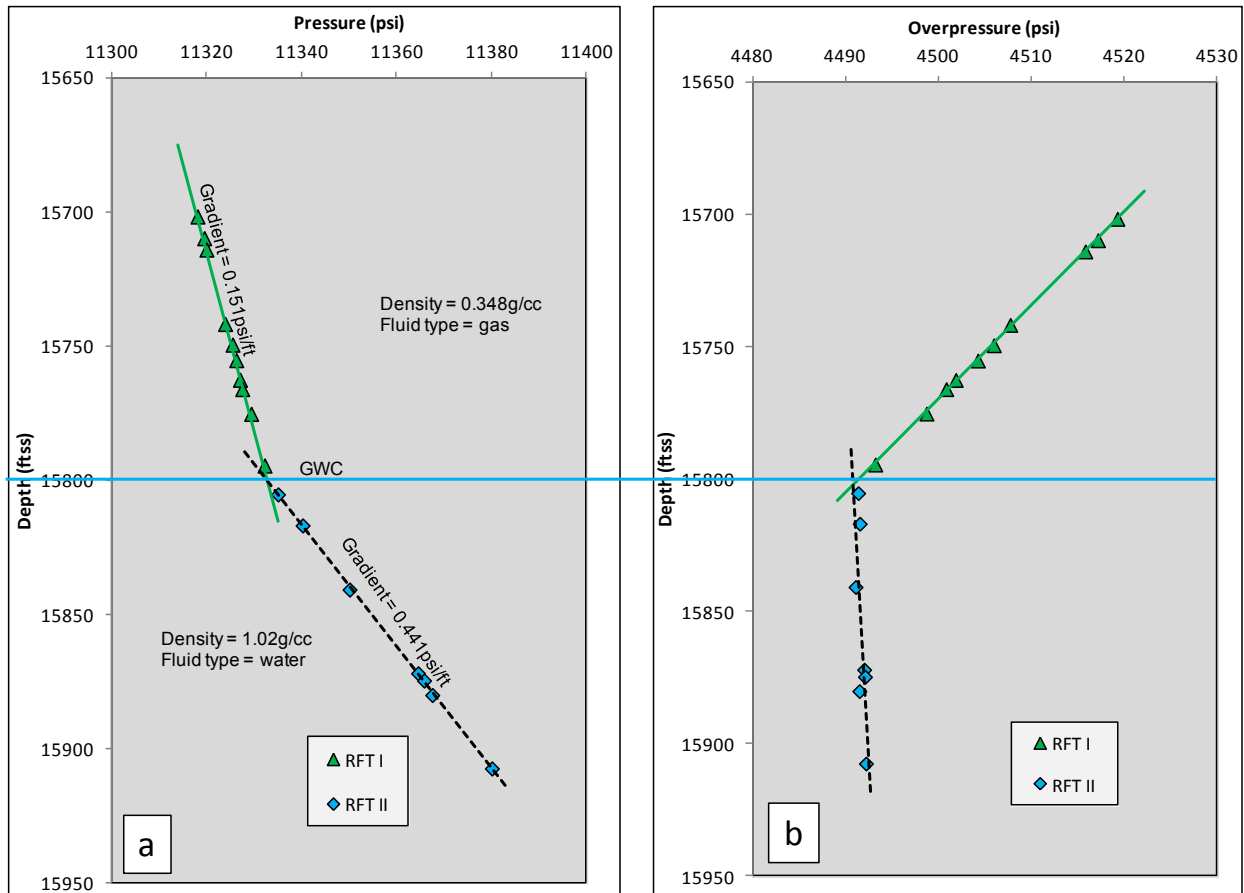

Figure 11 Depth plot of measured pressures and associated overpressures in deep reservoir (15700 ft - 15950ft). Overpressure in the water column is in excess of 4490psi (30.96MPa).

Figure 11 shows overpressure amounts calculated from pressure data obtained in the deep-seated reservoir interval below the massive shale at 14500ft (4421m) have two evident trends; an upper clockwise-rotated trend and a base relatively vertical trend (Figure 11b). These trends intersect at 15800ft (4817m) with corresponding slope inflection on the pressure-depth plot (Figure 11a). The gradient of the upper trend is 0.15psi/ft while the lower trend is 0.441psi/ft giving a corresponding density of 0.348g/cc and 1.02g/cc respectively. These fluids are interpreted as gas and water hence a gas-water contact (GWC) is delineated at 15800ft.

5. Discussion and conclusion

Analyses of wireline logs and measured reservoir pressure data in the Central Swamp Depobelt indicate a subsurface environment where high formation pressures may be due to the combined effects of disequilibrium compaction and late geopressuring processes such as hydrocarbon generation and associated diagenetic clay reactions. The petrophysics-based 1D pore pressure analysis was constrained with well data in the field. A large spread of observed gaps in logs (Figure 5) is probably caused by intervals where tools did not record data. However, the data spread and associated uncertainties were reasonably reduced after editing, integration and interpolation. Observed velocity reversal with relatively constant density (Figure 6) at certain depths indicates that overpressure could have clearly over-stepped the causative bounds of undercompaction mechanisms. This is also supported by the cross-plot of velocity and vertical effective stress (Figure 7a). Temperature regime calculated at the point of reversal approaches 120°C (Figure 7b), which indicates that the sediments are clearly within the hydrocarbon maturation window and diagenetic clay transformations. According to Hunt [13], the maturation of source rocks to oil and gas is a process that is driven by temperature and this optimally occurs at the range of 60°C to 120°C. The gas generating process may continue beyond this

range often reaching as high as 200°C. Evidence from cross-plot of rock properties and temperature regimes therefore support that hydrocarbon generation could be responsible for high overpressures experienced in deep settings of the field.

The iteration of geopressure profile derives from sonic velocity to pore pressure transform using routine Eaton, modified Eaton and Bowers methods (Figure 8).The application of Eaton exponent, n, value of 3.0 underestimated deep-seated overpressures by as much as 2391psi (16.49MPa) at 15803 ft (4818m) while an adjusted value of 5.5 produced a profile consistent with wireline pressure data. Loading curve parameters ($A = 0.3640$, $B = 0.977$) in Bowers method were determined by minimizing the difference between the estimated and actual effective stress. Pore pressures inside the velocity reversal were computed from the unloading curve relation with $U = 3.8$.

The nature and distribution of fluids in the reservoir was investigated by transforming wireline pressure data to overpressure magnitudes based on a normal hydrostatic pressure gradient of 0.4299 psi/ft determined in this study (Figure 3) which indicates fresh to near-normal marine salinity. Intervening succession of massive shales at an approximate depth of 14500 ft (4421m) partitions the reservoir system into an upper reservoir and lower reservoir. The upper reservoir (Figure 10) that lies above the massive shales is ineffectively overpressured with pressures in the water leg exceeding baseline hydrostatic values by as little as 150 psi (1.03MPa). Relying on trend inflections in depth plots of reservoir overpressures and pressure gradients, fluid variations were delineated based on density differences. Derived pressure gradients of 0.44 psi/ft, 0.298 psi/ft and 0.099 psi/ft were converted to densities as 1.01 g/cc, 0.69 g/cc and 0.23 g/cc corresponding to conventional water, oil and gas respectively. The resulting fluid densities indicate a distinct contact between water and hydrocarbons. Gas-oil-contact (GOC) occurred at 11500 ft (3506.1m) while oil-water-contact (OWC) is at 11650 ft (3552m).

The lower reservoir (Figure 11) that lies beneath the massive shale at depths greater than 14500ft (4421m) shows only two trends of wireline pressure data that intersect at approximately 15800 ft (4817.1m) with overpressure amounts that exceed 4490psi (30.96MPa). Gradients of the slopes in Figure 11 are 0.441psi/ft and 0. 151psi/ft which corresponds to densities values of 1.02g/cc and 0.348g/cc that is indicative of water and gas respectively. It is therefore interpreted that the slope inflexion point at 15800ft (4817m) is a gas-water-contact. Considering that oil phase could occupy a maximum of 150 ft (45.73m) in the upper reservoir and the ubiquitous distribution of gas in both reservoirs, the study well qualifies better as a gas well.

The massive shale at 14500ft (4421m) is a low permeability seal that effectively prevents pressure equilibration across the two reservoirs thus water saturated sections in both reservoirs are overpressured by different amounts despite being of the same fluid quality as shown by their densities. It is important to emphasise that severe drilling challenges occur close to or within the massive shale. Drilling through the thick shale zone and into the underlying potential hydrocarbon reservoir can be achieved with the use of advanced drilling technology and the better formulation of drilling fluids, capable of operating with minimal problems under these harsh conditions.

Acknowledgement

Reference

[1]   Athy, L.F., 1930. Density, porosity, and compaction of sedimentary rocks: American Association of Petroleum Geologists Bulletin, Vol. 14, P. 1-22.
[2]   Bowers G. L.,1995. Pore pressure estimation from velocity data: accounting for overpressure mechanisms besides under compaction. Society of Petroleum Engineers, Drilling and completion, P. 89-95.
[3]   Bowers, G. L., 2002. Detecting high overpressure. Applied Mechanics Technologies, Houston, Texas, U.S. The leading Edge, P.174-177.

[4]   Brown, A., 2003. Improved interpretation of wireline pressure data. AAPG Bulletin, v. 87, no. 2 (February 2003), pp. 295–311.

[5]   Corredor, F., Shaw, J.H., & Bilotti, F. 2005. Structural styles in the deep-water fold and thrust belts of the Niger Delta. *AAPG Bulletin, 89*, 753-780.

[6]   Chukwuma, M., Brunel, C., Cornu, T and Carre, G., 2013. Overcoming pressure limitations in Niger Delta Basin: Digging Deep into New Frontier on Block- X. Journal of Geology and Geosciences 2: 112. doi:10.4172/jgg.1000112.

[7]   Doust H., Omatsola E.,1990. Niger Delta, in *Divergent/passive Margin basins*, Edwards J.D., Santogrossi P.A. (eds), *AAPG Memoir* 45, 239-248.

[8]   Eaton, Ben. A., 1975. The equation for Geopressure Prediction from well logs, Paper 5544, Society of Petroleum Engineers, Texas.

[9]   Ejedawe, J., 2012. Nigeria Potential Waiting to be Tapped. AAPG Explorer, May 2012.

[10]   Engelder, T., 1993. Stress Regimes in the Lithosphere. Princeton University Press.

[11]   Gutierrez, Mario A., Braunsdort, Neil R., and Couzens Brent A. 2006. Calibration and ranking of pore-pressure prediction Shell International Exploration and Production, Houston, USA. The Leading Edge, P. 1516-1523.

[12]   Huffman, A. R, 2011. Recent advances in pore pressure prediction in complex geologic environment. Society of Petroleum Engineers Paper, Bahrain.

[13]   Hunt, J.M., 1996. Petroleum Geochemistry and Geology. 2nd Edition. W.H. Freeman, New York, 743pp.

[14]   Slotnick, M. M., 1936. On seismic computations, with applications II: Geophysics, Vol. 1, No. 3, P. 299-305.

[15]   Nwozor, K.K., Omudu, M.L., Ozumba, B.M., Egbuachor, C.J., and Odoh, B.I., 2012: A Relationship between Diagenetic Clay Minerals and Pore Pressures in an Onshore Niger Delta Field. Petroleum Technology Development Journal; July 2012 – Vol.2 (2).

[16]   O'Connor, Stephen A., Swarbrick, Richard E., Hoesni, M. J., and Lahann, R., 2011. Deep pore pressure prediction in challenging areas, Malay Basin, SE Asia, Proceedings of Indonesia Petroleum Association, 35th Annual Convention and Exhibition.

[17]   Swarbrick, R., O'Connor, S., and Lahann, R., 2005. Maximizing Geological Information from pressure tests and depth plots. Oil and Gas Journal v.103 (36).

[18]   Swarbrick, R.E., Osborne, M.J. & G.S. Yardley, 2002. Comparison of overpressure magnitude resulting from the main generating mechanisms. In: Huffman, A.R., Bowers, G.L. (eds), Pressure Regimes in Sedimentary Basins and their Prediction: *AAPG Memoir 76. pp. 1-12.*

[19]   Terzaghi, K., 1943. Theoretical Soil Mechanics, John Wiley and sons, New York.

[20]   Wawan A. Behaki, Aldyth Sukapradja, Ronald C. Siregar, Radig Wisnu Y, Setiabundi Djaelani, and Benny A. Sjafwan 2012. 3D Pore Pressure model in Bentu Block-central Sumatra Basin, Extended abstract AAPG International Convention and Exhibition, Singapore.

[21]   Weber, K.J., and Daukoru, E.M, 1975. Petroleum geology of the Niger Delta. Proceedings of 9th World Petroleum Congress. Tokyo 2 (Geology), 209 -221.

[22]   Yardley and Swarbrick, 2002. Lateral transfer: a source of additional overpressure?: Marine and Petroleum Geology, v.17, p.523-538.

[23]   Zhang, J., 2011. Pore pressure prediction from well logs: Methods, modifications, and new approaches. Earth Science Reviews 108: 50-63.